Engineering ORR Electrocatalysts from Co_8Pt_4 Carbonyl Clusters via ZIF-8 Templating

Peter M. Schneider,[a] Kathrin L. Kollmannsberger,[b] Cristiana Cesari,[c] Rachit Khare,[b] Maxime Boniface,[d] Beatriz Roldán Cuenya,[d] Thomas Lunkenbein,[d] Martin Elsner,[b] Stefano Zacchini,[c] Aliaksandr S. Bandarenka,*[a] Julien Warnan,*[b] and Roland A. Fischer*[b]

To reduce the costs of proton exchange membrane fuel cells, the amount of Pt necessary to drive efficient oxygen reduction reaction (ORR) should be minimized. Particle nanostructuring, (nano-)alloying, and metal-doping can yield higher activities per Pt mass through tailoring catalysts owning a high number of active sites and precise electronic properties. In this work, the atom-precise $[NBnMe_3]_2[Co_8Pt_4C_2(CO)_{24}]$ (**Co_8Pt_4**) cluster is encapsulated and activated in a zeolitic imidazolate framework (ZIF)-8, which unlocks the access to defined, bare Pt–Co nanoclusters, $Co_{8\pm x}Pt_{4\pm y}NC@ZIF-8$, for the fabrication of highly active ORR catalysts. Upon controlled C-interfacing and ZIF-8-digestion, Co-doped Pt NPs ($Pt_{27}Co_1$) with a homogenous and

narrow size distribution of (1.1 ± 0.4) nm are produced on Vulcan® carbon. Restructuring of the $Pt_{27}Co_1/C$ catalyst throughout the ORR measurement was monitored *via* high-angle annular dark field-scanning transmission electron microscopy and X-ray photoelectron spectroscopy. The measured ORR mass activity of (0.42 ± 0.07) Amg_{Pt}^{-1} and the specific activity of (0.67 ± 0.06) $mAcm_{ECSA}^{-2}$ compare favourably with the catalyst obtained by direct C-interfacing the pristine **Co_8Pt_4** cluster and with state-of-the-art Pt/C reference catalysts. Our results demonstrate the potential of ZIF-8-mediated Pt–Co NP synthesis toward devising ORR catalysts with high Pt-mass activity.

Introduction

As the awareness of climate change and its consequences grows, the rapid decoupling of the energy supply from fossil fuels becomes critical.[1] Research in developing and understanding nanostructured electrocatalysts is essential to improve energy conversion technologies, such as proton exchange membrane fuel cells (PEMFCs). The oxygen reduction reaction (ORR) at the cathode of PEMFCs is one of the most important and most widely studied electrocatalytic reactions to tackle the energy transition from fossil fuels to a hydrogen-based society.[2] However, sluggish ORR kinetics require the use of scarce and expensive noble metal catalysts, such as Pt, limiting the application of PEMFCs to date.[3] Therefore, increasing the catalyst's activity normalized to its Pt mass is becoming essential to cut costs and enable widespread use. One promising strategy to reach high Pt mass activity catalysts comprises nanoparticles due to their high surface-to-volume ratio allowing higher reaction rates compared to their bulk equivalents.[4] In addition, the nanostructuring of the catalyst significantly impacts the electrocatalytic ORR activity by varying the degree of active and coordinated sites.[5,6] Further, creating heterogeneous catalysts *via* adding non-noble transition metals can introduce strain and ligand effects which influence the electronic properties of the catalyst.[7] For instance, the binding of the reaction intermediate *OH during ORR can be weakened, resulting in increased catalytic activity.[8] Specifically, Pt and PtM NPs (M = e.g. Co, Ni) with a narrow size distribution in the lower nanometer range, homogeneously shaped and with precise stoichiometries,[5,9] have been identified as potential superior ORR catalysts compared to pure, regularly structured Pt.[10] A strong interest is paid to PtCo-based catalysts, with various academic and industrial examples having shown superior ORR catalytic activity.[11,12] Already low amounts of Co, down to doping levels, have been found to promote catalytic activity and stability.[13,14] While these results showcase the potential of

[a] P. M. Schneider,+ Prof. Dr. A. S. Bandarenka
Catalysis Research Center
Ernst-Otto-Fischer Straße 1, 85748, Garching, Germany
and
Department of Physics, TUM School of Natural Sciences
Technical University of Munich
James-Franck-Strasse 1, 85748, Garching, Germany
E-mail: bandarenka@ph.tum.de

[b] K. L. Kollmannsberger,+ Dr. R. Khare, Prof. Dr. M. Elsner, Dr. J. Warnan, Prof. Dr. R. A. Fischer
Catalysis Research Center
Ernst-Otto-Fischer Straße 1, 85748, Garching, Germany
and
Department of Chemistry, TUM School of Natural Sciences
Technical University of Munich
Lichtenbergstraße 4, 85748, Garching, Germany
E-mail: roland.fischer@tum.de
        julien.warnan@tum.de

[c] Dr. C. Cesari, Prof. Dr. S. Zacchini
Dipartimento di Chimica Industriale "Toso Montanari"
Università di Bologna
Viale del Risorgimento 4, 40136 Bologna, Italy

[d] Dr. M. Boniface, Prof. Dr. B. Roldán Cuenya, Prof. Dr. T. Lunkenbein
Department of Interface Science
Fritz Haber Institute of the Max Planck Society
Faradayweg 4–6, 14195 Berlin, Germany

nanostructured PtCo materials, the synthesis and the understanding of their high activity remain modest, with structure-activity relationships being rarely investigated.[12]

The precise synthesis of Pt_xCo_y NPs in the lower nanometer size (1–2 nm) is intrinsically difficult as their high density of low coordination sites creates a strong driving force toward agglomeration.[12,15] A distinct metal ratio and NP size are often compromised by Co leaching, especially during electrocatalysis, rendering a precise Pt_xCo_y stoichiometry control highly challenging.[12] Typically, extremely sophisticated, controlled and non-scalable approaches (e.g., high vacuum setups) are employed for fabricating defined NPs.[15–17] A different synthetic strategy, however, envisions using small metal nanoclusters (NCs; ≤1 nm) as atom-precise precursors for tailor-made NPs.[18] These defined NCs are stabilized by a ligand shell and synthesized wet-chemically, avoiding energy-intensive vacuum procedures.[19] Yet, their capping ligands restrict the access of reactants and impact the electronic properties. Removing the ligands often proceeds under harsh conditions, which promotes aggregation processes.[19,20] Ligand-stripping while cluster core retainment constitutes a major challenge.

Metal-organic frameworks (MOFs) as 3D, stable, crystalline and porous matrices can be employed as stabilizing scaffolds to carry and host different species,[21] including metal NPs[22] and ligand-stabilized clusters.[23,24] A highly suitable MOF is the zeolitic imidazolate framework (ZIF)-8, which is known for its formation under mild conditions, scaffolding of pore-size exceeding species, as well as for its stability and carrier ability.[25] For instance, $[Pt_9(CO)_{12}](NBu_4)_2$, a reactive, atom-precise cluster, was successfully ZIF-8 encapsulated. The subsequent ligand-removal yielded bare, ZIF-8-confined Pt NCs close to its original nuclearity,[24] which serve as precursor to fabricate Pt NPs of 1.10 ± 0.17 nm with a high Pt mass activity in the ORR.[9] Despite the potential of MOF-hosted atom-precise clusters as template for active ORR, no other similar material has been investigated so far.

Recently, we report on the *bottle-around-ship* encapsulation of a series of preformed mixed metal carbonyl nanoclusters, e.g. $[NBnMe_3]_2[Co_8Pt_4C_2(CO)_{24}]$ (**Co₈Pt₄**), in ZIF-8.[26] Herein, we report on **Co₈Pt₄@ZIF-8** as a potential bimetallic electrocatalyst precursor (Scheme 1). The ZIF-8 encapsulated **Co₈Pt₄** was activated *via* decarbonylation yielding "naked", pore-confined clusters,[26] which were in turn released out the ZIF-8 matrix generating Pt_xCo_y NPs supported on Vulcan® carbon for electrocatalytic ORR. A rotating disc electrode (RDE) setup is used to determine the ORR activity, which was found to increase throughout the electrochemical measurement. This could be correlated to the catalyst restructuring by employing high-angle annular dark field (HAADF)-scanning transmission electron microscopy (STEM) and X-ray photoelectron spectroscopy (XPS). During electrochemical cycling, partial Pt reduction and controlled NP growth of the Pt_xCo_y NPs yielded the final stable and active catalyst species. The determined ORR mass activity of (0.42 ± 0.07) A mg_{Pt}^{-1} and specific activity of (0.67 ± 0.06) mA cm_{ECSA}^{-2} of the obtained material outperforms that of the directly deposited **Co₈Pt₄** cluster and competes with state-of-the-art commercial Pt/C catalysts.

Results and Discussion

$Co_{8\pm x}Pt_{4\pm y}NC@ZIF-8$ is exploited as a precursor to form Pt_xCo_y NPs *via* the *bottle-around-ship* approach.[26] Vulcan® XC72R serves as a catalyst support material to test the activity of Pt_xCo_y NPs toward the ORR. 9.0 mg of the carbon support was interfaced with the 18 mg $Co_{8\pm x}Pt_{4\pm y}NC@ZIF-8$ by first dispersing them individually in 3.5 mL of MeOH *via* sonication. Secondly, both suspensions are combined, again sonicated, and the solvent is removed in a dynamic vacuum yielding $Co_{8\pm x}Pt_{4\pm y}NC@ZIF-8/C$. Powder X-ray diffractometry (PXRD), scanning electron microscopy (SEM), and transmission electron microscopy (TEM) were used to assess the mixing behavior and
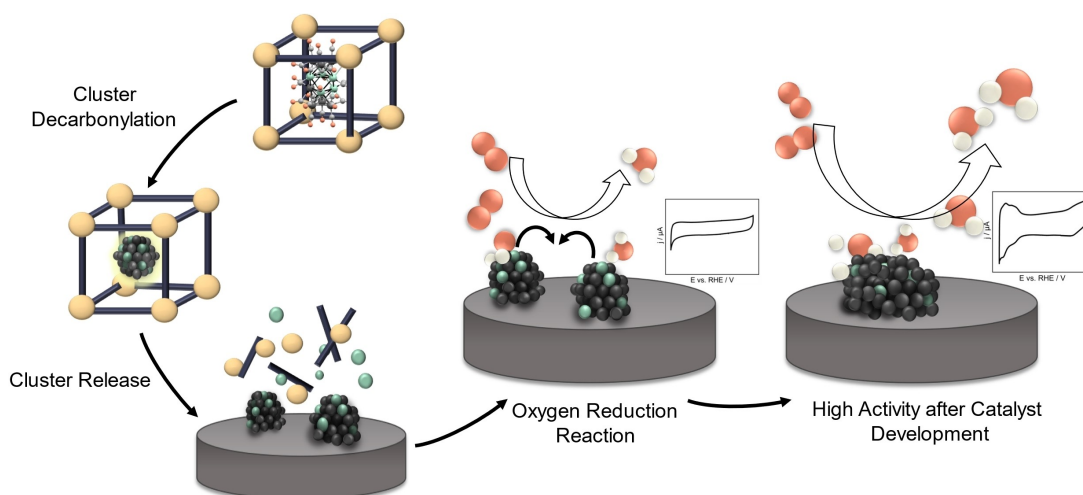
Scheme 1. Schematic overview of the catalyst synthesis procedure: **Co₈Pt₄@ZIF-8** acts as a precursor for generating bare $Co_{8\pm x}Pt_{4\pm y}NC@ZIF-8$ *via* cluster decarbonylation. Acid-induced cluster release yields precise Pt-enriched PtCo NPs as electrocatalysts for the ORR. Catalyst development throughout the measurement leads to increased ORR activity.

ChemElectroChem

Research Article
doi.org/10.1002/celc.202300476

**Chemistry
Europe**
European Chemical
Societies Publishing

interaction between C and $Co_{8\pm x}Pt_{4\pm y}NC$@ZIF-8. The PXRD mainly reveals ZIF-8-related reflections with an amorphous, C-like background (Figure 1a).[27] The TEM image in Figure 1b depicts particles which are assignable to C[28] and to $Co_{8\pm x}Pt_{4\pm y}NC$@ZIF-8,[26] exemplarily marked with arrows and circles, respectively. However, due to the similar particle size of C[29] (Figure S1**c**) and $Co_{8\pm x}Pt_{4\pm y}NC$@ZIF-8[26] (d~20 nm), the two components are challenging to differentiate, especially in the SEM images (Figure S1). Thus, the same hybridization synthesis was repeated using ZIF-8 particles with a diameter of ~100 nm yielding ZIF-8/C (ZIF-8 synthesis details in the experimental part). Now, the SEM images reveal an effective mixing (Figure S1d, e) which in turn suggests a concurrent behavior for $Co_{8\pm x}Pt_{4\pm y}NC$@ZIF-8/C.

Changing the $Co_{8\pm x}Pt_{4\pm y}NC$@ZIF-8 to C ratio provides an opportunity to vary the loading of the active catalyst material on the carbon support, which depicts a crucial feature in electrocatalysis to optimize the catalytic behavior depending on the desired use. Increasing the ratio from 2 to 4 adds up to the higher relative intensity of the ZIF-8 diffraction pattern (Figure S2). To release the nanoclusters from the ZIF-8 cage, $Co_{8\pm x}Pt_{4\pm y}NC$@ZIF-8/C composites were exposed to an aqueous solution of 1.0 M AcOH for 2 h to achieve quantitative ZIF-8 digestion. After washing and drying, the Pt_xCo_y/C powder was obtained and further characterized.

PXRD only revealed carbon-related reflections as Pt(Co) reflections were not visible, likely due to the highly dispersed, nanoscale-size and low amount of encapsulated and then released NPs (Figure 1a).[27] HAADF-STEM images show that the NPs are distributed homogeneously on the carbon support resulting in effective utilization of the active catalyst material (Figure 2 and Figure S3). Figure 2b depicts a magnified view of the catalyst nanoparticles with a substantial number of single atoms attached to the carbon support alongside narrow size-distributed NPs with a mean diameter of ~ (1.1 ± 0.4) nm (Figure S3). This demonstrates the potential of the MOF-mediated *bottle-around-ship* approach toward producing precise NPs.[24] The metal composition of the synthesized PtCo NPs was quantified *via* inductively coupled plasma mass spectrometry (ICP-MS), revealing a Pt loading of (3.5 ± 0.6) wt.-% with a low Co content of (0.05 ± 0.01) wt.-%. X-ray emission spectroscopy (XES) measurements were performed to assess the Co content and its oxidation state in our Pt_xCo_y NPs. The amount of Co in the Pt_xCo_y/C catalyst is estimated to be ~0.06 wt.-% based on the intensity of the edge-jump (relative to that in the **Co_8Pt_4@ZIF-8** sample) observed in the Co $K\alpha_1$ high energy resolution fluorescence detected (HERFD) X-ray absorption spectra (see Figure 2c). In addition, the edge position in XANES indicates that Co, in the Pt_xCo_y/C catalyst, is present in an oxidized state. This leads to a metal stoichiometry of averaged **$Pt_{27}Co_1$/C** with the Pt enrichment compared to **Co_8Pt_4** being attributed to a Co leaching mediated by protons[12] and 2-MeIm[30] in the course of the ZIF-8 digestion. Utilizing the precursor $Co_{8\pm x}Pt_{4\pm y}NC$@ZIF-8 with a higher metal loading of 5.3 compared to 3.5 wt.-% Pt or as well using a higher $Co_{8\pm x}Pt_{4\pm y}NC$@ZIF-8 to C ratio (4:1 instead of 2:1) resulted in higher Pt/Co content of 6.6/0.06 and 6.0/0.05 wt.-%, respectively. This underlines the adjustability of the synthesis approach.

XPS analysis, presented in Figure 2d, shows the fitted spectrum of the Pt 4f core level and suggests the presence of oxidized Pt species (Pt $4f_{7/2}$ at 72.8 and 75.2 eV assigned to Pt-II and -IV, respectively)[31] in the NPs. This is in accordance with the tendency of small Pt particles to oxidize easily.[29] Figure S4 displays the fitted spectra of the Co 2p core-level region of $Pt_{27}Co_1$/C for two individual measurements. The sharp peaks located at 781.4 eV (Figure S4a) and 781.1 eV (Figure S4b) can be assigned to the Co $2p_{3/2}$ core-levels of Co-II. This reveals that not only Pt is present in an oxidized form, but also Co. An overview of the location of the binding energies for the fitted Co and Pt core-level regions is available in Table S1. From the fitted spectra it is obvious that the Pt 4f and Co 2p peaks are shifted up to ~0.4 and ~1.5 eV to higher binding energies, respectively. The increase in binding energy of the Pt 4f[13,32] and Co 2p[33] core-level regions has already been associated with the alloying between Pt and Co in numerous works due to a downshift of the d-band center as a result of the electronic interaction of Pt and Co upon alloying. This is a strong hint that Co is present in an alloyed form in our catalyst system. It is important to note that other phenomena, such as the particle-
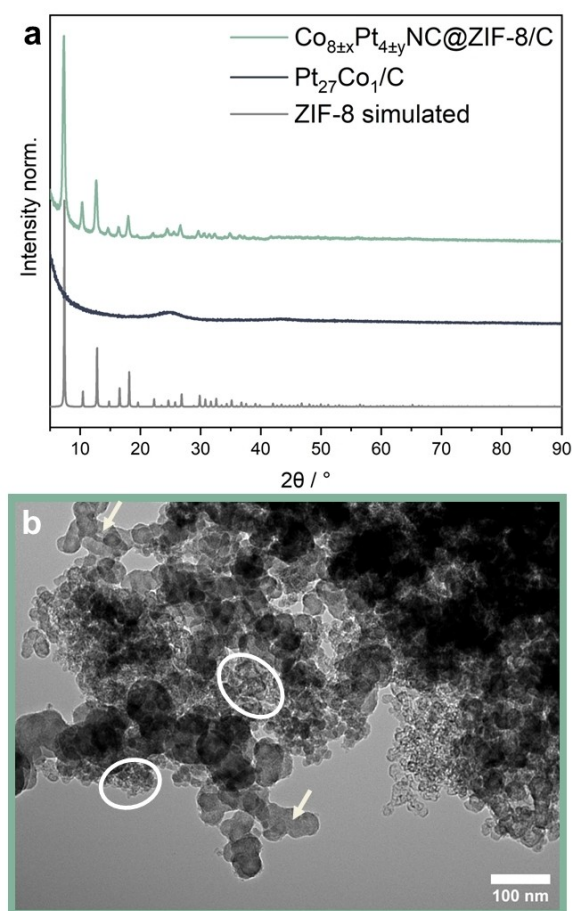

Figure 1. (**a**) PXRD and (**b**) TEM of $Co_{8\pm x}Pt_{4\pm y}NC$@ZIF-8. White arrows and circles mark exemplarily particles which are assigned to C and $Co_{8\pm x}Pt_{4\pm y}NC$@ZIF-8, respectively. The PXRD after the acidic MOF digestion yielding $Pt_{27}Co_1$/C is shown in (**a**) and compared to a simulated ZIF-8 pattern.[30]

ChemElectroChem
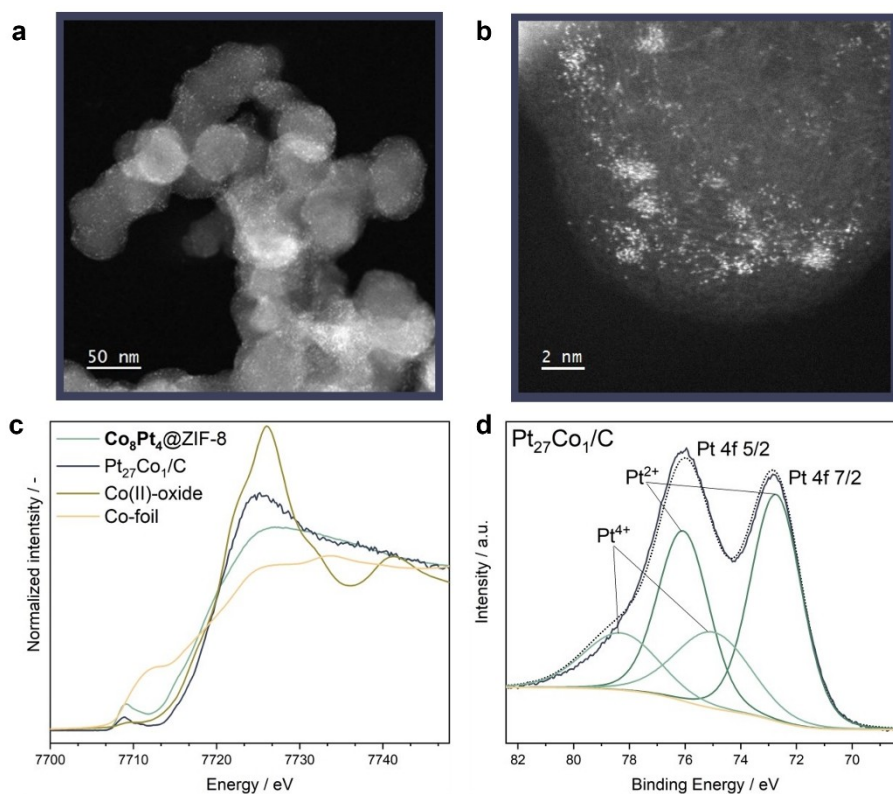
Research Article
doi.org/10.1002/celc.202300476

**Chemistry
Europe**
European Chemical
Societies Publishing

Figure 2. (**a**) HAADF-STEM image of the $Pt_{27}Co_1/C$ electrocatalyst before electrochemical examination. (**b**) Zoomed-in view of single Pt atoms dispersed on Vulcan® carbon support. (**c**) Co K_α HERFD XANES of Co_8Pt_4@ZIF-8 and $Pt_{27}Co_1/C$. The XANES of Co(II)-oxide and Co-foil are also shown for comparison. (**d**) Fitted XPS spectrum of the Pt 4f core-level region of $Pt_{27}Co_1/C$ directly after the synthesis.

size effect[34] or interactions with the carbon support,[35] can also lead to a shift of the core-level peaks to higher binding energies. However, the influence of metal-support interactions on the XPS core-levels is small for amorphous carbons, such as Vulcan® XC72R, used in this work[36] and was not observed in the C 1s nor in the N 1s XPS spectra (Figure S5 and S6).

As mentioned previously, size-precise Pt nanoparticles doped with small amounts of Co have shown superior ORR activity.[13,14] To assess the catalytic performance of our derived bimetallic PtCo composite, a water/isopropanol-based ink containing $Pt_{27}Co_1/C$ composite and Nafion™ was evaluated toward ORR by RDE measurements in acidic media (0.1 M $HClO_4$, pH~1) and compared to commercial Pt/C catalysts commonly used in literature. The Pt loading on the glassy carbon RDE tip was calculated to be 3.5 $\mu g\,cm^{-2}$. A Pt wire and a mercury-mercurous sulfate electrode were used as counter and reference electrode, respectively. A typical cyclic voltammogram (CV) of the electrochemical examination of the $Pt_{27}Co_1/C$ catalyst in Ar-saturated 0.1 M $HClO_4$ is shown in Figure 3a. Typical Pt features, such as the H-adsorption/-desorption peaks or oxide-formation/-reduction peaks, were not observed in the first cycle (dark blue curve). This might be attributed to either the low Pt weight loading of our $Pt_{27}Co_1/C$ catalyst or the potential blockage of its surface, so that little to no species can be adsorbed to the active Pt, and the CV is dominated by the capacitive behavior of the carbon support. The presence of predominantly Pt-II and -IV species instead of metallic Pt could

also contribute to the missing Pt features in the CV in Ar atmosphere. While cycling between 0.1 and 1.0 V vs reversible hydrogen electrode (RHE) is known to clean, activate and stabilize the catalyst surface, typically shown by, i.e., formation and stabilization of H-adsorption/-desorption or oxide-formation/-reduction peaks over several cycles, this was not observed in our case even after a several dozen cycles.[37] The dotted curve in Figure 3b displays an exemplary anodic scan of the ORR polarization curve of $Pt_{27}Co_1/C$ in O_2-saturated 0.1 M $HClO_4$ between 0.1 and 1.0 V vs RHE directly after the electrochemical activation. With continuous cycling under ORR conditions, the electrocatalytic performance of $Pt_{27}Co_1/C$ improved, which is evident from the shift of the polarization curve toward more positive potentials instead of stabilizing or deteriorating, as typically observed during ORR. After several hundred cycles (solid curve in Figure 3b), the polarization curve stabilizes and does not change further. The ORR onset potential increased from ~0.85 to 0.96 V vs RHE, while the current density at 0.9 V vs RHE increased from ~0.16 to 1.46 mA cm_{geo}^{-2} and the half-wave potential $\Delta E_{1/2}$ shifted by almost 100 mV. Following the last ORR polarization curve, we again recorded CVs in Ar-saturated 0.1 M $HClO_4$ to further examine the observed activity increase. In contrast to prior catalyst testing, characteristic Pt features, such as H-adsorption/-desorption peaks between ~0.06 and 0.30 V vs RHE, as well as oxide-formation/-reduction peaks of Pt between ~0.7 and 1.0 V vs RHE were now visible (orange curve in Figure 3a). These observations support that
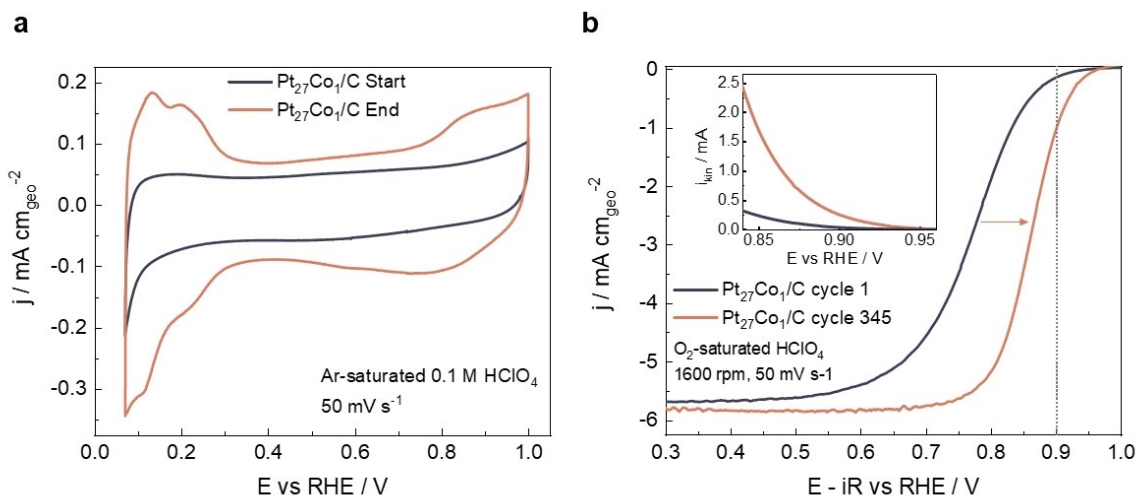
ChemElectroChem

Research Article
doi.org/10.1002/celc.202300476

Chemistry Europe
European Chemical
Societies Publishing

Figure 3. (a) Typical CVs of $Pt_{27}Co_1/C$ in Ar-saturated 0.1 M $HClO_4$ at a scan rate of 50 mV s^{-1} in the beginning (dark blue curve) and in the end (orange curve) of the electrochemical examination, normalized to the geometric surface area of the glassy carbon electrode (0.196 cm^2). (b) Typical *iR*-drop-corrected anodic ORR polarization curves of $Pt_{27}Co_1/C$ in O_2-saturated 0.1 M $HClO_4$ at a rotation speed of 1600 rpm and scan rate of 50 mV s^{-1}, normalized to the geometrical surface area of the glassy carbon electrode. Pseudocapacitive currents were corrected by subtraction of a background CV recorded in Ar atmosphere. The corresponding kinetic current curves in a potential range around 0.9 V vs RHE are displayed in the inset.

the main active species likely developed throughout the electrochemical examination over up to 1000 cycles. This can be explained by an increase in either the number of available active sites for the ORR or the intrinsic activity of the $Pt_{27}Co_1/C$ catalyst material through NP size and shape alteration during cycling (compare Figures 2a and 4a). Here, it is important to note that the activation of the catalyst and its activity increase is neither dependent on O_2- or Ar-saturation nor on the counter electrode material or the cycling potential window (Figure S7). From the CVs in Ar atmosphere after electrochemical cycling for up to 1000 cycles, we calculated a specific surface area (SSA) of 51 ± 11 m^2 g$_{Pt}^{-1}$ based on hydrogen underpotential deposition (HUPD) as these CVs should represent the real catalyst surface after the electrochemical activation.

HAADF-STEM images recorded after the extensive electro-chemical cycling process (Figure 4a and Figure S8) reveal larger, but still narrowly size-distributed NPs with a calculated mean diameter of $\sim(2.05 \pm 0.66)$ nm homogeneously distributed on the carbon support. Concomitantly, fewer single atoms can be observed. The dissolution of less stable single atoms, migration, and coalescence or Ostwald ripening during the electrochem-ical cycling could have induced the growth of the initial NPs until they reach an energetically stable state.[16,38,39] The distinct NP formation is in accordance with the post-catalysis fitted XPS spectrum of the Pt 4f core-level region revealing the presence of Pt^0 (Pt $4f_{7/2}$ at 71.3 eV, Figure 4b).[31] The presence of the metallic Pt^0 after the electrochemical measurements, in contrast to mainly oxidized Pt species before, could contribute to more pronounced Pt features observed in Figure 3a and a higher
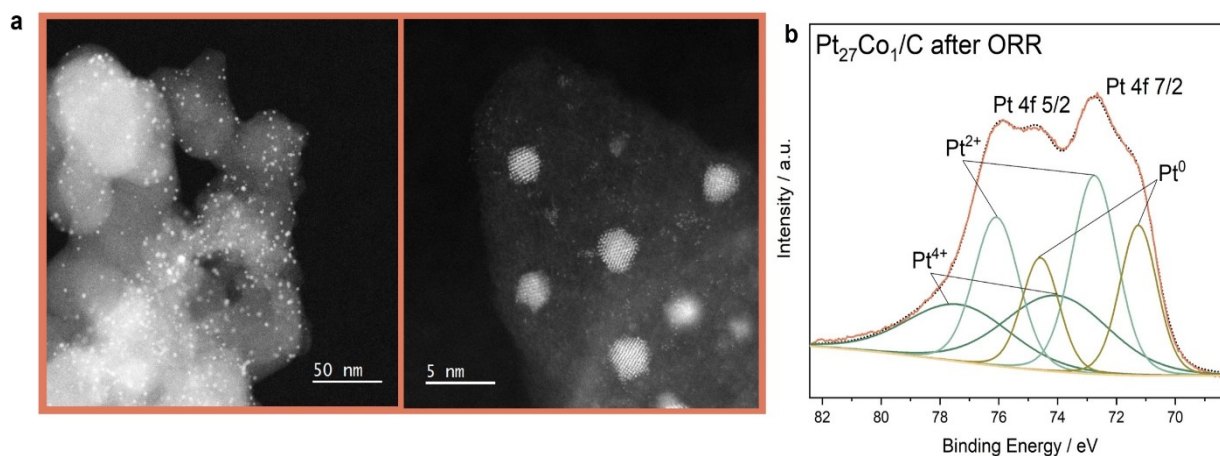

Figure 4. (a) HAADF-STEM images of the $Pt_{27}Co_1/C$ electrocatalyst after electrochemical examination for up to 1000 cycles in O_2-saturated 0.1 M $HClO_4$. (b) Fitted XPS spectrum of the Pt 4f core-level region of $Pt_{27}Co_1/C$ after ~1000 ORR cycles.

ChemElectroChem

Research Article
doi.org/10.1002/celc.202300476

Chemistry
Europe
European Chemical
Societies Publishing

onset potential of the ORR polarization curve in Figure 3b. Continuous cycling of the catalyst thus leads to better utilization of Pt in the form of enlarged, partially reduced NPs exposing more active metallic Pt compared to the initially predominant Pt oxide species and single atoms.[31,39,40] ICP-MS of the catalytic layer and electrolyte post-cycling further revealed that half of the Co leached out during the measurement, leaving low amounts of Co incorporated in the actual catalytic species.

The inset in Figure 3b underlines the dramatic increase in ORR performance of the $Pt_{27}Co_1/C$ during electrochemical cycling by displaying the increase in kinetic current, calculated from the ORR polarization curve, between 0.85 and 0.95 V vs RHE. The kinetic current after the aforementioned electrochemical activation of $Pt_{27}Co_1/C$, normalized to the mass of active Pt catalyst material, yields a mass activity as high as (0.42 ± 0.07) A mg_{Pt}^{-1}. A more detailed look at the evolution of ORR polarization curves for two individual measurements is shown in Figures S10a and b. They reveal that the strongest increase in performance happens within the first ~100 cycles, which can also be seen by the steep increase of the MA in Figure S10b. Furthermore, Figures S9 and S10 indicate a stable catalyst system as the MA stays constant for ~500 cycles until a decay in the polarization curve and the MA is noticeable. While this testing duration indicates good catalyst stability, prolonged testing in membrane electrode assemblies is required for a "real-life" endurance assessment. The mass activity evaluated for our $Pt_{27}Co_1/C$ catalyst is comparable to that of the state-of-the-art commercial Pt/C catalyst produced by Tanaka (TKK, 20 wt.-%, mass activity ~0.42 A mg_{Pt}^{-1}) reported by Fichtner et al.[41] The specific activity (SA) of $Pt_{27}Co_1/C$ of (0.67 ± 0.06) mA cm_{ECSA}^{-2}, evaluated by normalizing the kinetic current at 0.9 V vs RHE to the ECSA, is even slightly higher than that reported by Fichtner et al. (~0.61 mA cm_{ECSA}^{-2}).[41] Comparing the MA of our Co-doped Pt/C catalyst with the average stoichiometry $Pt_{27}Co_1/C$ with other PtCo/C catalyst systems from the literature shows the success of this work as it can compete with other catalysts and even outperform most. Table S2 and Figure S11 give an overview of various Pt/C and PtCo/C catalysts found in the literature. Our catalyst also outperforms various other commercially available Pt/C catalysts (TKK, E-TEK, HiSPEC), even reaching double the mass and specific activity (Figure 5).[13,42]

Finally, to investigate the role of the MOF scaffolding, the performance of the MOF-derived $Pt_{27}Co_1/C$ catalyst was compared to that of the MOF-free heterogenized **Co₈Pt₄** cluster. Vulcan® XC72R was impregnated with a MeOH solution of the **Co₈Pt₄** nanocluster, dried and activated via ligand removal at 200 °C under dynamic vacuum (5.4 wt.-% Pt, 2.8 wt.-% Co, $Co_1Pt_{0.57}/C$). Again, no Pt(Co) NP reflections could be found in the PXRD pattern (Figure S12). TEM images reveal small NPs which are narrowly size distributed $((1.1 \pm 0.4)$ nm) but heterogeneously dispersed over the carbon support and showing less single atoms (Figure S13). Applying this composite in the electrochemical measurements showed only a slight activity improvement throughout the electrochemical activation procedure. However, compared to the MOF-derived $Pt_{27}Co_1/C$ it
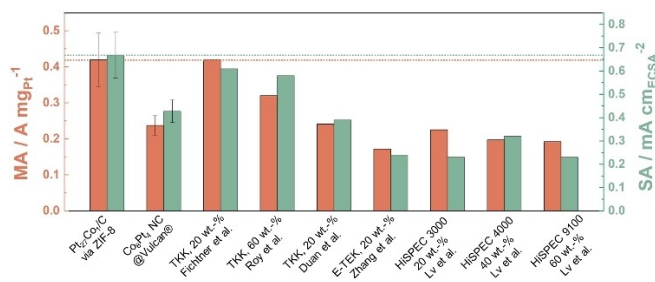

Figure 5. Mass activity (MA) and specific activity (SA) of $Pt_{27}Co_1/C$ via ZIF-8 encapsulation versus direct deposition of the metal nanocluster on carbon ("Co_8Pt_4 NC/Vulcan®") evaluated at 0.9 V vs RHE in 0.1 M $HClO_4$ at a rotation speed of 1600 rpm. MA and SA values of commercial Pt/C Tanaka, E-TEK, and HiSPEC Pt/C catalysts are added from the literature to compare the ORR activity of $Pt_{27}Co_1/C$ via ZIF-8 catalyst synthesized in this work with state-of-the-art Pt/C catalysts. Dotted orange and green lines mark the highest mass and specific activity, respectively, achieved among the ORR catalysts presented here.

reaches a lower final mass activity of (0.24 ± 0.03) A mg_{Pt}^{-1} (see Figure 5 and Figure S14), half that of $Pt_{27}Co_1/C$. This points towards advantages brought by the encapsulation of the metal nanocluster toward defined high-performing catalysts.

Conclusions

Here, an atom-precise carbonyl cluster, $[NBnMe_3]_2[Co_8Pt_4C_2(CO)_{24}]$, functions as Pt–Co NP precursor via ZIF-8-hosting. After cluster activation, $Co_{8\pm x}Pt_{4\pm y}NC@ZIF-8$ is interfaced with the nanostructured carbon support. An efficient interfacing and adjustable $Co_{8\pm x}Pt_{4\pm y}NC@ZIF-8$ to C ratio allows to obtain homogenously distributed and narrow-size $Pt_{27}Co_1$ NPs with adjustable Pt-loading. RDE experiments revealed a high catalytic ORR mass activity after the catalyst developed throughout the electrochemical measurement. This is associated with nanoparticle restructuring and oxidation state changes. The catalytic performance surpasses commercial Pt/C catalysts as well as the directly deposited **Co₈Pt₄** cluster.

The lower activity of the latter can mainly be attributed to the composition and the significantly more inhomogeneous PtCo NP distribution with fewer sub-nanometer species. However, the role of the Co content in the catalyst has not been elucidated yet, while previous publications about $Pt_{36}Co/C$ materials attributed their superior activity to the Co-leached surface structure and electronic effects next to the small size and the homogenous NP dispersion.[14] Classic approaches in metallurgy typically yield larger NPs with an alloyed Pt core surrounded by a pure Pt shell, which serves as the electrochemically active layer due to the shape defects introduced by leaching of the non-noble metal.[43] In contrast, our synthetic route utilizing the *bottle-around-ship* encapsulation of atom-precise **Co₈Pt₄** clusters in ZIF-8 specifically aimed to creating defined Pt NPs doped with small amounts of Co to obtain the same effect of shape defects of a core-shell NP. By this we could simulate the effect of the active Pt shell without wasting the scarce catalyst material of the alloyed NP core. Nevertheless,

ChemElectroChem

Research Article
doi.org/10.1002/celc.202300476

Chemistry Europe
European Chemical
Societies Publishing

the higher Co content compared to the MOF-derived PtCo NPs demonstrate the necessity of optimizing the digestion procedure, cluster release and deposition toward maintaining the initial cluster nuclearity. This would allow to assess the influence of the Co content better and increase the benefits of the MOF-mediated synthesis approach against the straight cluster deposition further.

This study facilitates the journey towards atom-precise cluster-MOF composites generating nanostructured and transition metal-doped ORR catalysts with high activity and minimum Pt content for PEMFCs.

Experimental

$Co_{8\pm x}Pt_{4\pm y}NC@ZIF-8/C$: 18.0/36.0 mg of $Co_{8\pm x}Pt_{4\pm y}NC@ZIF-8$ and 9.00 mg carbon black (Vulcan®XC72R) were dispersed in 3.5 mL MeOH *via* ultrasonication, mixed again through sonification and dried *in vacuo* yielding a black powder.

ZIF-8: 775 mg 2-methylimidazole (9.44 mmol, 7.04 eq.) dissolved in 10 mL MeOH were combined with a solution of 350 mg of $Zn(NO_3)_2 \cdot 4H_2O$ (1.34 mmol, 1.00 eq.) in 10 mL MeOH at 50 °C. After stirring for 5 min, aging for 10 min, centrifugation, washing with THF (3×10 mL) and drying in dynamic vacuum 66 mg of the white powder was obtained (0.29 mmol, 22%).

$Pt_{27}Co_1/C$ $(Co_{8\pm x}Pt_{4\pm y}NC@ZIF-8$ derived): 20 mg of $Co_{8\pm x}Pt_{4\pm y}NC@ZIF-8/C$ was immersed in 5 mL of 1.0 M AcOH for 2 h and subsequently washed with H_2O (2×5 mL) and dried in dynamic vacuum.

$Co_1Pt_{0.57}/C$ *(direct cluster deposition):* 2.6 mg of $[NBnMe_3]_2[Co_8Pt_4C_2(CO)_{24}]$ dissolved in 2 mL MeOH was mixed with 20 mg C (Vulcan®XC72R) suspended in 5 mL MeOH. The solvent was removed under a dynamic vacuum while stirring. The dried powder was heated to 200 °C under a dynamic vacuum for 2 h utilizing a sand bath yielding a black powder.

Ink preparation

For the RDE measurements, 2 mg of the catalyst material were dispersed in 713 µL of ultra-pure water, 289 µL isopropanol and 6 µL of Nafion, and sonicated for 20–30 min. 10 µL of this suspension were deposited on a polished glassy carbon electrode and dried under continuous rotation at 300 rpm to obtain a homogeneous catalyst coating. Prior to the electrochemical measurements, the glassy carbon tip was polished with 1, 0.3, and 0.05 µm alumina paste, respectively, and rinsed with ultra-pure water. From the Pt weight loading of the catalyst, the volume of drop-casted ink, and the geometrical surface of the glassy carbon (0.196 cm²), the Pt loading per cm² on the glassy carbon RDE tip was calculated.

Conflict of Interests

The authors declare no conflict of interest.

Data Availability Statement

The data that support the findings of this study are available from the corresponding author upon reasonable request.

[1] W. Steffen, K. Richardson, J. Rockström, S. E. Cornell, I. Fetzer, E. M. Bennett, R. Biggs, S. R. Carpenter, W. de Vries, C. A. de Wit, et al., *Science* **2015**, *347*, 1259855.

[2] X. Tian, X. F. Lu, B. Y. Xia, X. W. Lou, *Joule* **2020**, *4*, 45.

[3] a) S. Sui, X. Wang, X. Zhou, Y. Su, S. Riffat, C.-j. Liu, *J. Mater. Chem. A* **2017**, *5*, 1808; b) H. A. Gasteiger, S. S. Kocha, B. Sompalli, F. T. Wagner, *Appl. Catal. B* **2005**, *56*, 9.

[4] a) M. K. Debe, *Nature* **2012**, *486*, 43; b) N. Jung, D. Y. Chung, J. Ryu, S. J. Yoo, Y.-E. Sung, *Nano Today* **2014**, *9*, 433.

[5] M. Rück, A. Bandarenka, F. Calle-Vallejo, A. Gagliardi, *Nanoscale Adv.* **2019**, *1*, 2901.

[6] F. Calle-Vallejo, M. D. Pohl, D. Reinisch, D. Loffreda, P. Sautet, A. S. Bandarenka, *Chem. Sci.* **2017**, *8*, 2283.

[7] a) S. Zaman, L. Huang, A. I. Douka, H. Yang, B. You, B. Y. Xia, *Angew. Chem.* **2021**, *60*, 17832; b) B. Garlyyev, J. Fichtner, O. Piqué, O. Schneider, A. S. Bandarenka, F. Calle-Vallejo, *Chem. Sci.* **2019**, *10*, 8060.

[8] a) J. Greeley, I. E. L. Stephens, A. S. Bondarenko, T. P. Johansson, H. A. Hansen, T. F. Jaramillo, J. Rossmeisl, I. Chorkendorff, J. K. Nørskov, *Nat. Chem.* **2009**, *1*, 552; b) R. M. Kluge, R. W. Haid, A. Riss, Y. Bao, K. Seufert, T. O. Schmidt, S. A. Watzele, J. V. Barth, F. Allegretti, W. Auwärter et al., *Energy Environ. Sci.* **2022**, *15*, 5181.

[9] B. Garlyyev, K. Kratzl, M. Rück, J. Michalička, J. Fichtner, J. M. Macak, T. Kratky, S. Günther, M. Cokoja, A. S. Bandarenka et al., *Angew. Chem.* **2019**, *58*, 9596.

[10] a) X. Wang, Z. Li, Y. Qu, T. Yuan, W. Wang, Y. Wu, Y. Li, *Chem* **2019**, *5*, 1486; b) V. Čolić, A. S. Bandarenka, *ACS Catal.* **2016**, *6*, 5378.

[11] T. Yoshida, K. Kojima, *Electrochem. Soc. Interface* **2015**, *24*, 45.

[12] H. Chen, J. Liu, X. Wu, C. Ye, J. Zhang, J.-L. Luo, X.-Z. Fu, *Small* **2022**, *18*, e2204100.

[13] X. Duan, F. Cao, R. Ding, X. Li, Q. Li, R. Aisha, S. Zhang, K. Hua, Z. Rui, Y. Wu et al., *Adv. Energy Mater.* **2022**, *12*, 2103144.

[14] X. Tang, D. Fang, L. Qu, D. Xu, X. Qin, B. Qin, W. Song, Z. Shao, B. Yi, *Chin. J. Catal.* **2019**, *40*, 504.

[15] K. Wettergren, F. F. Schweinberger, D. Deiana, C. J. Ridge, A. S. Crampton, M. D. Rötzer, T. W. Hansen, V. P. Zhdanov, U. Heiz, C. Langhammer, *Nano Lett.* **2014**, *14*, 5803.

[16] J. Quinson, M. Röefzaad, D. Deiana, T. W. Hansen, J. B. Wagner, M. Nesselberger, A. S. Crampton, C. J. Ridge, F. F. Schweinberger, U. Heiz et al., *Electrochim. Acta* **2018**, *277*, 211.

[17] K. Yamamoto, T. Imaoka, *Acc. Chem. Res.* **2014**, *47*, 1127.

[18] a) Z. W. Seh, J. Kibsgaard, C. F. Dickens, I. Chorkendorff, J. K. Nørskov, T. F. Jaramillo, *Science* **2017**, *355*; b) F. Baletto, *J. Phys. Condens. Matter* **2019**, *31*, 113001; c) A. S. Crampton, M. D. Rötzer, C. J. Ridge, F. F. Schweinberger, U. Heiz, B. Yoon, U. Landman, *Nat. Commun.* **2016**, *7*,

10389; d) T. Kawawaki, Y. Kataoka, M. Hirata, Y. Iwamatsu, S. Hossain, Y. Negishi, *Nanoscale Horiz.* **2021**, *6*, 409.

[19] H. Rong, S. Ji, J. Zhang, D. Wang, Y. Li, *Nat. Commun.* **2020**, *11*, 5884.

[20] C. Cesari, J.-H. Shon, S. Zacchini, L. A. Berben, *Chem. Soc. Rev.* **2021**, *50*, 9503.

[21] a) Y. Shu, Q. Ye, T. Dai, Q. Xu, X. Hu, *ACS Sens.* **2021**, *6*, 641; b) T. H. Bennett, M. D. Vaughn, S. A. Davari, K. Park, D. Mukherjee, B. Khomami, *Nanoscale Adv.* **2019**, *1*, 94.

[22] a) C. Gao, F. Lyu, Y. Yin, *Chem. Rev.* **2021**, *121*, 834; b) K. L. Kollmannsberger, L. Kronthaler, J. R. Jinschek, R. A. Fischer, *Chem. Soc. Rev.* **2022**, *51*, 9933.

[23] a) S. Ji, Y. Chen, Q. Fu, Y. Chen, J. Dong, W. Chen, Z. Li, Y. Wang, L. Gu, W. He et al., *J. Am. Chem. Soc.* **2017**, *139*, 9795; b) Y. Luo, S. Fan, W. Yu, Z. Wu, D. A. Cullen, C. Liang, J. Shi, C. Su, *Adv. Mater.* **2018**, *30*, 1704576–1704576; c) L. Sun, Y. Yun, H. Sheng, Y. Du, Y. Ding, P. Wu, P. Li, M. Zhu, *J. Mater. Chem. A* **2018**, *6*, 15371; d) Y. Zhu, X. Qiu, S. Zhao, J. Guo, X. Zhang, W. Zhao, Y. Shi, Z. Tang, *Nano Res.* **2020**, *13*, 1928; e) K. L. Kollmannsberger, K. Weger, T. Kratky, S. Günther, O. Tomanec, J. Warnan, R. A. Fischer, *Mol. Syst. Des. Eng.* **2021**, *6*, 876; f) F. Zheng, Y. Fan, W. Chen, *ACS Appl. Mater. Interfaces* **2021**, *13*, 38170.

[24] K. Kratzl, T. Kratky, S. Günther, O. Tomanec, R. Zbořil, J. Michalička, J. M. Macak, M. Cokoja, R. A. Fischer, *J. Am. Chem. Soc.* **2019**, *141*, 13962.

[25] a) Y. Pan, Y. Liu, G. Zeng, L. Zhao, Z. Lai, *Chem. Commun.* **2011**, *47*, 2071; b) S. Mallakpour, E. Nikkhoo, C. M. Hussain, *Coord. Chem. Rev.* **2022**, *451*, 214262.

[26] K. L. Kollmannsberger, Poonam, C. Cesari, R. Khare, T. Kratky, M. Boniface, O. Tomanec, J. Michalička, E. Mosconi, A. Gagliardi, et al., *Chem. Mater.* **2023**, *35*, 5475.

[27] A. Bayrakçeken, A. Smirnova, U. Kitkamthorn, M. Aindow, L. Türker, İ. Eroğlu, C. Erkey, *Chem. Eng. Commun.* **2008**, *196*, 194.

[28] M. Klingenhof, P. Hauke, S. Brückner, S. Dresp, E. Wolf, H. N. Nong, C. Spöri, T. Merzdorf, D. Bernsmeier, D. Teschner et al., *ACS Energy Lett.* **2021**, *6*, 177.

[29] A. Eguizabal, L. Uson, V. Sebastian, J. L. Hueso, M. P. Pina, *RSC Adv.* **2015**, *5*, 90691.

[30] Y. Yun, H. Sheng, K. Bao, L. Xu, Y. Zhang, D. Astruc, M. Zhu, *J. Am. Chem. Soc.* **2020**, *142*, 4126.

[31] A. S. Aricò, A. K. Shukla, H. Kim, S. Park, M. Min, V. Antonucci, *Appl. Surf. Sci.* **2001**, *172*, 33.

[32] a) B. P. Vinayan, R. Nagar, N. Rajalakshmi, S. Ramaprabhu, *Adv. Funct. Mater.* **2012**, *22*, 3519; b) T. Yang, H. Zhu, M. Wan, L. Dong, M. Zhang, M. Du, *Chem. Commun.* **2016**, *52*, 990; c) S. Axnanda, K. D. Cummins, T. He, D. W. Goodman, M. P. Soriaga, *ChemPhysChem* **2010**, *11*, 1468; d) M. Wakisaka, S. Mitsui, Y. Hirose, K. Kawashima, H. Uchida, M. Watanabe, *J. Phys. Chem. B* **2006**, *110*, 23489.

[33] a) S.-I. Choi, S.-U. Lee, W. Y. Kim, R. Choi, K. Hong, K. M. Nam, S. W. Han, J. T. Park, *ACS Appl. Mater. Interfaces* **2012**, *4*, 6228; b) H. Zhao, Z.-P. Hu, Y.-P. Zhu, L. Ge, Z.-Y. Yuan, *Chin. J. Catal.* **2019**, *40*, 1366.

[34] a) W. Eberhardt, P. Fayet, D. M. Cox, Z. Fu, A. Kaldor, R. Sherwood, D. Sondericker, *Phys. Rev. Lett.* **1990**, *64*, 780; b) T. T. P. Cheung, *Surf. Sci.* **1984**, *140*, 151; c) G. K. Wertheim, S. B. DiCenzo, S. E. Youngquist, *Phys. Rev. Lett.* **1983**, *51*, 2310.

[35] X. Ge, F. W. T. Goh, B. Li, T. S. A. Hor, J. Zhang, P. Xiao, X. Wang, Y. Zong, Z. Liu, *Nanoscale* **2015**, *7*, 9046.

[36] a) G. Gupta, D. A. Slanac, P. Kumar, J. D. Wiggins-Camacho, J. Kim, R. Ryoo, K. J. Stevenson, K. P. Johnston, *J. Phys. Chem. C* **2010**, *114*, 10796; b) Y. Lou, J. Xu, Y. Zhang, C. Pan, Y. Dong, Y. Zhu, *Mater. Today Nano* **2020**, *12*, 100093.

[37] R. M. Arán-Ais, Y. Yu, R. Hovden, J. Solla-Gullón, E. Herrero, J. M. Feliu, H. D. Abruña, *J. Am. Chem. Soc.* **2015**, *137*, 14992.

[38] Y. Shao-Horn, W. C. Sheng, S. Chen, P. J. Ferreira, E. F. Holby, D. Morgan, *Top. Catal.* **2007**, *46*, 285.

[39] K. Hartl, M. Nesselberger, K. J. J. Mayrhofer, S. Kunz, F. F. Schweinberger, G. Kwon, M. Hanzlik, U. Heiz, M. Arenz, *Electrochim. Acta* **2010**, *56*, 810.

[40] K. J. J. Mayrhofer, S. J. Ashton, J. C. Meier, G. K. H. Wiberg, M. Hanzlik, M. Arenz, *J. Power Sources* **2008**, *185*, 734.

[41] J. Fichtner, B. Garlyyev, S. Watzele, H. A. El-Sayed, J. N. Schwämmlein, W.-J. Li, F. M. Maillard, L. Dubau, J. Michalička, J. M. Macak, et al., *ACS Appl. Mater. Interfaces* **2019**, *11*, 5129.

[42] a) C. Roy, B. P. Knudsen, C. M. Pedersen, A. Velázquez-Palenzuela, L. H. Christensen, C. D. Damsgaard, I. E. L. Stephens, I. Chorkendorff, *ACS Catal.* **2018**, *8*, 2071; b) M. Zhang, Y. Dai, J.-Y. Hu, S. Miao, B.-Q. Xu, *J. Phys. Chem. C* **2021**, *125*, 27199; c) Y. Lv, H. Liu, J. Li, J. Chen, Y. Song, *J. Electroanal.* **2020**, *870*, 114172.

[43] a) J. Fichtner, S. Watzele, B. Garlyyev, R. M. Kluge, F. Haimerl, H. A. El-Sayed, W.-J. Li, F. M. Maillard, L. Dubau, R. Chattot, et al., *ACS Catal.* **2020**, *10*, 3131; b) E. B. Tetteh, C. Gyan-Barimah, H.-Y. Lee, T.-H. Kang, S. Kang, S. Ringe, J.-S. Yu, *ACS Appl. Mater. Interfaces* **2022**, *14*, 25246.